CarbonPump: Mathematics of the SuTiT flexible inner tube for efficient soil core sampling

Melanie E. Roberts[1] Fillipe Georgiou[2]
Edward J Bissaker[3] Barry J. Cox[4] James M. Hill[5]
Michael H. Meylan[6] Josiah Murray[7]
Winston L. Sweatman[8] Ngamta Thamwattana[9]

Received 20 December 2022

Abstract

Soil core samples underpin the evaluation of soil carbon stocks, an essential measurement to enable and support the establishment and operation of soil carbon natural capital markets. Soil cores are obtained by driving a tube as far as 1500 mm into the ground to extract a vertically profiled sample. Robust, reusable sampling devices are essential to minimise sampling costs while reducing waste. The SuTiT is a customised inner tube designed to reduce waste while supporting rapid sampling across various dryland soils, including sandy and clay

DOI:10.21914/anziamproc.v64.20044, Published 2025-08-25, as part of the Proceedings of the Mathematics in Industry Study Group. ISSN 1445-8810.

soils, which present unique challenges for extracting an intact core. The SuTiT provides for a flexible inner tube that, when closed, can be easily inserted into the solid outer tube and, when removed, relaxes naturally into a trough shape for easy access to the sample. A combination of kerf cuts and presses is used to achieve these features. This study group focussed on opportunities to increase the shelf-life of the SuTiT through exploration of the kerf patterns and their effect on the strength and bending properties of the tube.

1 Introduction and Problem Description

Soil core sampling is an important tool to support agriculture, infrastructure, and land and environmental management decision making. Analysis of soil core samples is used to understand soil profiles and properties, soil nutrient profiles, and root mass. The role of soil organic carbon, the largest pool of terrestrial carbon [3], in combating climate change has recently gained increased attention. Soil core sampling is one method by which carbon assessments are undertaken [2]. Consequently, the growth of natural capital markets for soil organic carbon will likely see an expansion in soil assessments via core sampling.

Soil cores are typically collected by driving a cylindrical tube up to 1500 mm into the ground. When extracted, this provides a soil sample across multiple soil horizons. There are many complexities in sampling soil cores. A sampling rig must be suitable to obtain samples in a variety of soil types and properties, including sandy soils (which risk falling out of the tube as extracted), clays (which when wet stick to the inner walls of the tube), and rocks (which are difficult to penetrate with the corer). Furthermore, sampling speed (including the processing of samples) affects the cost of obtaining samples.

Although there is some variety in approaches, in dry land conditions, typically, two approaches are used to collect soil samples. In the first approach, a single-walled tube is driven into the ground and withdrawn. In the second approach, a pipe with an inner tube is used and the inner tube is extracted

with the sample for processing. In both cases, the tubes are forced into the ground using a combination of force (hydraulic ram and mass) and impact (jackhammer). The pros and cons of these two approaches depend on the sampling depth, the accessibility of the sampling site, and the soil composition at different depths.

CarbonPump, an Australian soil carbon company, favour the double-tube approach for ease of deployment in the field. They investigated several approaches before custom-developing the SuTiT, a flexible, removable steel inner tube. The advantages of the SuTiT over alternatives include ease of use in the field, both for the deployment and processing of samples, and for the reduction in waste over single-use options. Improving the lifespan of the SuTiT device will further reduce landfill waste and reduce manufacturing costs, further improving the cost-benefit of this approach.

The SuTiT (Figure 1.1) is a steel inner tube and consists of three axial and five radial regions. The base (and top) of the SuTiT has a series of rectangular cutouts spaced around the radius. These cutouts anchor the SuTiT to the collar, preventing it from moving within the outer tube during deployment or extraction. A soil retainer is placed between the collar and the SuTiT to prevent the samples from falling during extraction. The central region of the SuTiT, which occupies most of the length, is a combination of pressed and kerf-cut regions.

At rest, the SuTiT has a natural trough or U-shape, achieved through cold presses at approximately 1/3 and 2/3 along the short axis creating the corners (Figure 1.1). Kerf cuts are used at the edges and centre to provide flexibility. This combination allows the SuTiT to be easily bent into a roughly circular shape for insertion into the outer tube while returning to the trough shape on extraction for ease of access to the core sample.

Although the SuTiT meets the operational requirements of CarbonPump, they have observed opportunities for improvement. The lifespan of the SuTiT is unpredictable due to failure or fracture when under load, which compromises the cost-effectiveness of the product. Furthermore, the laser-cut kerf regions

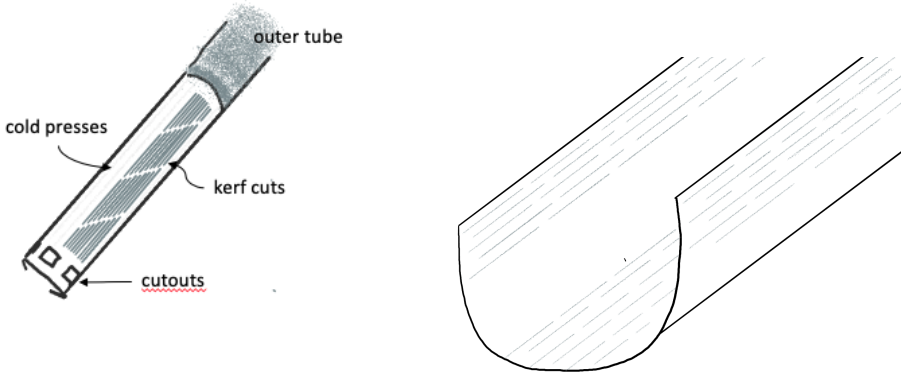

Figure 1.1: Schematic of the SuTiT inner liner. The figure on the left shows the SuTiT inserted into the outer tube (viewed from above). The figure on the right shows a slice of the SuTiT to illustrate the locations of the kerfed region. Cold presses are used to bend the flat metal sheet into the U-shape at rest. Kerfing (indicated by the grey lines) on the upper edges and along the base of the tube provide flexibility. The kerf pattern indicated is illustrative only.

account for the majority of the production costs. As the kerf-cut approach has been explored by trial and error, CarbonPump is interested in understanding if design improvements could improve durability and reduce production costs.

This MISG focused on understanding the mechanical properties of the SuTiT to improve the design to increase the lifespan. Specifically, we investigated

- the trade-offs between flexibility and strength of the SuTiT given the combination of cold press (plastic bend) and kerf cut (elastic bend) regions; and
- the implications of the kerf pattern on the strength, flexibility and durability.

2 A simple linear model

Consider a cross-section of the SuTiT to understand the role of the kerfed regions on the final shape of the tube when inserted into the outer tube. The one-dimensional Euler–Bernolli equation is used to model the deviation of the rest shape of the SuTiT when a force is applied to the edges to close the tube.

We use the standard calculus of variations formulation and let the shape of the tube be $\hat{S}(x)$, where x is distance around the tube. Assuming small deformations from the at-rest shape, energy E is related to the variation in the shape of the tube by,

$$E = \int_0^L D(x) \left(\frac{\partial^2 \hat{S}}{\partial x^2} \right)^2 dx, \tag{2.1}$$

for a given stiffness coefficient $D(x)$. The desirable solution is one for which the shape minimises the energy. Consider a variation in the shape such that

$$\hat{S}(x) = S(x) + \varepsilon h(x), \tag{2.2}$$

for some function $h(x)$ that vanishes at $x = 0$ and $x = L$ and also has a vanishing derivative at these points. The standard in the calculus of variations is to assume that $S(x)$ is the minimum energy solution and derive the appropriate equation. Introducing (2.2), and differentiating with respect to ε gives

$$\frac{\partial E}{\partial \varepsilon} = \int_0^L 2D(x) \left(\frac{\partial^2 S}{\partial x^2} + \varepsilon \frac{\partial^2 h}{\partial x^2} \right) \frac{\partial^2 h}{\partial x^2} \, dx. \tag{2.3}$$

The minimum energy state occurs when $\frac{\partial E}{\partial \varepsilon}\big|_{\varepsilon=0} = 0$, thus

$$\int_0^L D(x) \frac{\partial^2 h}{\partial x^2} \frac{\partial^2 S}{\partial x^2} \, dx = 0. \tag{2.4}$$

We model the variable stiffness of the SuTiT by considering a piece-wise approximation of N sections from x_{i-1} to x_i. Each section is assumed to have

constant stiffness $D(x) = D_i$. Exploiting the symmetry of the SuTiT about $x = 0$ and considering only the right-hand branch $0 \leqslant x \leqslant L$, then (2.4) can be approximated by

$$\sum_{i=0}^{N-1} D_i \int_{x_i}^{x_{i+1}} \frac{\partial^2 h_i}{\partial x^2} \frac{\partial^2 S_i}{\partial x^2} \, dx = 0, \tag{2.5}$$

where $x_0 = 0$ and $x_N = L$. Integrating (2.5) by parts twice gives

$$\sum_{i=0}^{N-1} D_i \left(\left[\frac{\partial h_i}{\partial x} \frac{\partial^2 S_i}{\partial x^2} \right]_{x_i}^{x_{i+1}} - \left[h_i \frac{\partial^3 S}{\partial x^3} \right]_{x_i}^{x_{i+1}} + \int_{x_i}^{x_{i+1}} h_i \frac{\partial^4 S_i}{\partial x^4} \, dx \right) = 0. \tag{2.6}$$

Applying the force F_a to the ends of the tube to bend it towards a circular shape results in a deformation $S(x)$ described by (2.6) and

$$D_N \frac{\partial^3 S_N}{\partial x^3} \bigg|_{x=L} = F_a, \tag{2.7}$$

and if there is no bending moment at the end

$$D_N \frac{\partial^2 S_N}{\partial x^2} \bigg|_{x=L} = 0. \tag{2.8}$$

Continuity in the zeroth and first derivatives in $S(x)$ and $h(x)$ at the knots $x = \{x_i \mid i \neq (0, N)\}$, requires that

$$S_i(x_i) = S_{i+1}(x_i), \quad \frac{\partial S_i}{\partial x} \bigg|_{x=x_i} = \frac{\partial S_{i+1}}{\partial x} \bigg|_{x=x_i}, \quad i = 1, \ldots, N-1, \tag{2.9}$$

$$h_i(x_i) = h_{i+1}(x_i), \quad \frac{\partial h_i}{\partial x} \bigg|_{x=x_i} = \frac{\partial h_{i+1}}{\partial x} \bigg|_{x=x_i}, \quad i = 1, \ldots, N-1, \tag{2.10}$$

and to anchor the shape at the origin and impose symmetry, it is necessary that

$$S(0) = 0, \tag{2.11}$$

and (2.12)

$$\left.\frac{\partial S}{\partial x}\right|_{x=0} = 0. \tag{2.13}$$

Since (2.6) must be true for all functions $h(x)$, we require

$$D_i \int_{x_i}^{x_{i+1}} h_i \frac{\partial^4 S_i}{\partial x^4} dx = 0, \quad i = 1, \ldots, N-1, \tag{2.14}$$

and that the force and bending moments match at each knot, i.e.

$$D_i \left[\frac{\partial^2 S_i}{\partial x^2}\right]_{x_i} = D_{i+1} \left[\frac{\partial^2 S_{i+1}}{\partial x^2}\right]_{x_i}, i = 1, \ldots, N-1, \tag{2.15}$$

and

$$D_i \left[\frac{\partial^3 S_i}{\partial x^3}\right]_{x_i} - D_{i+1} \left[\frac{\partial^3 S_{i+1}}{\partial x^3}\right]_{x_i} = 0, \quad i = 1, \ldots, N-1. \tag{2.16}$$

Expanding the solution in each region of constant stiffness as a third-order polynomial gives

$$S_i(x) = \sum_{j=0}^{3} c_{i,j} x^j. \tag{2.17}$$

This leads to a system of linear equations that must be solved for the coefficients $c_{i,j}$ derived from conditions (2.7 – 2.13), (2.15) and (2.16). This gives two conditions at $i = 0$ and $i = N$ and the four conditions at each of $i = 1, \ldots, N-1$. For example, if the plate is divided into three sections we have 12 unknowns and require 12 equations. These come from the 8 continuity equations for $i = 1, 2$ and the two end conditions at each of $x = 0$ and $x = L$.

The prototype SuTiT consists of five sections, as shown by the blue and black regions in Figure 2.1. Since we are modelling only half of the tube using

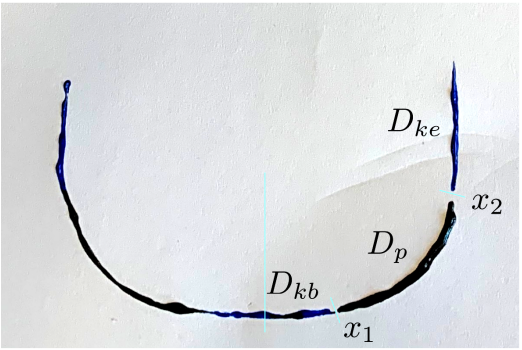

Figure 2.1: Geometry of the SuTiT in the relaxed state. x_1 and x_2 are the locations of transitions from kerfed (blue) to pressed (black) regions, measured from the centre of the SuTiT (line of symmetry). The stiffness coefficients of the three regions are indicated.

symmetry, we only have three regions. The trough or U-shape is achieved by cold presses at the bend, with kerfing at the edges and centre of the tube providing flexibility. We consider three stiffness coefficients D_{kb} in the centre kerfed region $0 \leqslant x < x_1$, D_p for the cold-pressed region $x_1 \leqslant x < x_2$, and D_{ke} for the kerfed edge region $x_2 < x \leqslant L$. This allows different kerf patterns to be used in the centre and edge regions. In this case we find the exact solution:

$$S(x) = \begin{cases} S_1(x), & 0 \leqslant x < x_1, \\ S_2(x), & x_1 \leqslant x < x_2, \\ S_3(x), & x_2 \leqslant x \leqslant L, \end{cases} \tag{2.18}$$

where

$$S_1(x) = \frac{F_a}{6D_{kb}}x^3 - \frac{F_a(L + x_1 - x_2)}{2D_{kb}}x^2, \tag{2.19}$$

$$S_2(x) = \frac{F_a}{6D_p}x^3 - \frac{F_a L}{2D_p}x^2 - \frac{F_a}{2}\left[\frac{1}{D_p}(x_1 - 2L) + \frac{1}{D_{kb}}(x_1 - 2x_2 + 2L)\right]x$$

$$+\frac{F_a x_1^2}{6}\left[\frac{1}{D_p}(2x_1-3L)+\frac{1}{D_{kb}}(x_1-3x_2+3L)\right], \quad (2.20)$$

and

$$S_3(x)=\frac{F_a}{6D_{ke}}x^3-\frac{F_aL}{2D_{ke}}x^2-\frac{F_a}{2}\left\{\frac{1}{D_{kb}}x_1(x_1-2x_2+2L)\right.$$
$$\left.+\frac{1}{D_p}\left[x_1^2-x_2^2+2L(x_2-x_1)\right]+\frac{1}{D_{ke}}x_2(x_2-2L)\right\}x$$
$$+\frac{F_a}{6}\left\{\frac{1}{D_{kb}}x_1^2(x_1-3x_2+3L)+\frac{1}{D_p}\left[x_1^2(2x_1-3L)+x_2^2(3L-2x_2)\right]\right.$$
$$\left.\frac{1}{D_{ke}}x_2^2(2x_2-3L)\right\}. \quad (2.21)$$

Thus, the resulting shape of the SuTiT after applying a small deformation due to the force F_a is given by $S_r(x)=S_0(x)+S(x)$, where $S_0(x)$ is the initial shape before the deformation.

To compare the results of linear theory with observations, we digitised the curves of SuTiT under various degrees of manual bending according to the method detailed in the next section. The rest state obtained by this approach is used as the initial shape $S_0(x)$ for this analysis.

2.1 Digitising SuTiT curvature for comparison with the mathematical model

For qualitative testing of the mathematical models developed in this paper, having digital constructions of the curvature of the SuTiT liner is convenient.

Our process for digitising the curvature of the liner was as follows.

Step 1: Coat the bottom edge of the liner in acrylic paint such that the kerfed and cold-pressed sections are blue and black, respectively.

Step 2: Press the bottom edge of the liner onto a sheet of copy paper to create an impression of the curvature.

Step 3: Photograph the impression using a standard mobile phone camera.

Step 4: Import the image into Webdigitizer (https://apps.automeris.io/wpd/).

Step 5: Using Webdigitizer, manually plot points marking the ends of the curve, the transition points between the kerfed and pressed sections, two midpoints along each kerfed section, and one midpoint along each pressed section.

Step 6: Import the coordinates of these points into MATLAB and use the native spline function to fit a curve.

The curvature was recorded under four conditions: rest state, partial closure under manual effort, complete closure under manual effort, and complete closure whilst within the external cylinder. Initial impressions are shown in Figure 2.2 and the final MATLAB plots in Figure 2.3. Curvature vectors, calculated by fitting a circle to the three neighbouring points (which is why there is no curvature vector for the last points) were added to Figure 2.3. The curvature vector for a point on a curve points to the centre of a circle best approximating the curve near the point. The magnitude of the vector is the curvature, which is the inverse of the circle's radius. This figure clearly shows the problem with the design. The curvature of the tube, even in the outer tube, is near zero at the ends. Elsewhere, the curvature is close to constant, showing the design is working well in those regions.

2.2 Results and Discussion

Using this model we applied a small deformation to the SuTiT in it's resting state to understand the effect of various parameter combinations. Comparison of the linear results with the observed shape under manual bending (Figure 2.4) demonstrates that this model is suitable to represent the resulting shape. The manual bending of the SuTiT involves the application of a force that changes

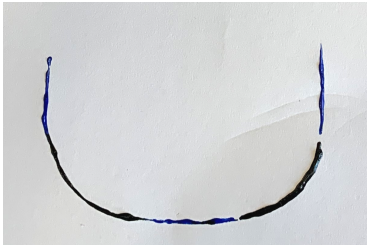

(a) Rest state

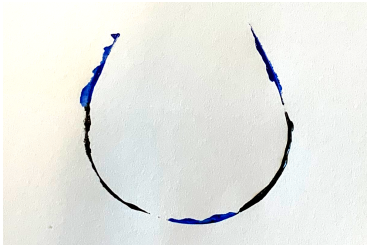

(b) Partial closure under manual effort

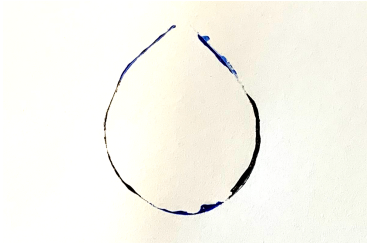

(c) Complete closure under manual effort

(d) Complete closure in external cylinder

Figure 2.2: Prints created during step 2 of the digitisation process.

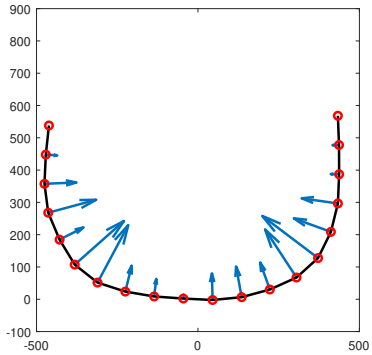

(a) Rest state

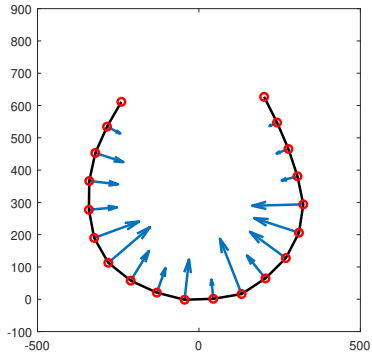

(b) Partial closure manual effort

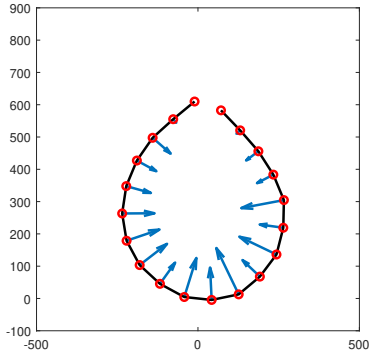

(c) Complete closure manual effort

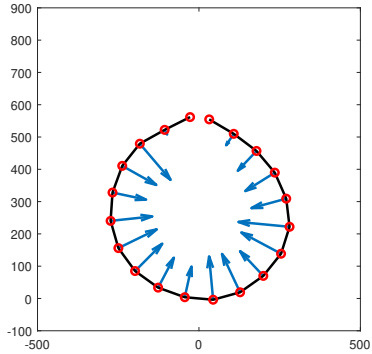

(d) Complete closure in external cylinder

Figure 2.3: Plots created during step 6 of the digitisation process, with vectors showing the magnitude and direction of the curvature.

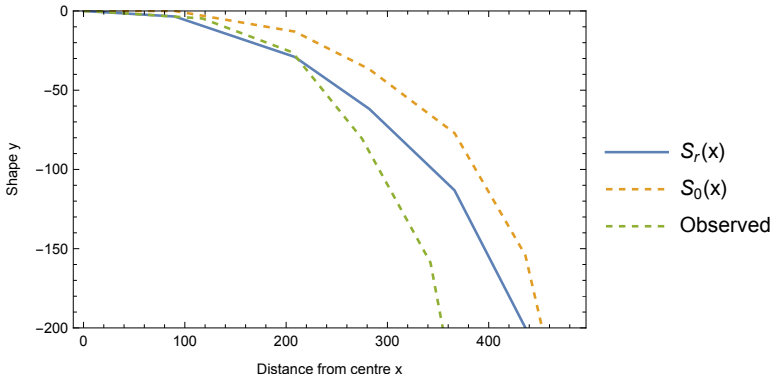

Figure 2.4: Resulting deformation of the SuTiT under an applied force according to the linear theory, with $x_1 = 143.089$, $x_2 = 594.37$, $F_a = 0.00024$, $D_{kb} = D_{ke} = 119$ and $D_p = 1440$. The dashed lines show the rest state (Figure 2.3a) and under partial closure (Figure 2.3b).

direction as it is bent. Consequently, linear theory with a uniform force applied to the ends illustrates only the first stage of bending. Nevertheless, this model illustrates several key properties of the SuTiT that are further explored in Figures 2.5 and 2.6.

The flexibility of the SuTiT is due more to the stiffness of the base kerfed region than the edge stiffness (Figure 2.5). Lower stiffness coefficients (Figure 2.5), and a wider base kerfed region (Figure 2.6A) both result in more significant deviation from the rest state under the same applied force. Minimal improvement is evident from a decreased edge stiffness (Figure 2.5B) or increased width (Figure 2.6B) for this region. These results show that the near linear shape observed on manually bending the SuTiT, see Figures 2.2 and 2.3, cannot be overcome by changes in the stiffness or location of the kerfed regions. This near linear region prevents the SuTiT from curving with the shape of the outer tube, resulting in a pressure point in the centre of the trough at $x = 0$. Modest increases to the stiffness at the edges may provide a more robust inner tube that is less prone to fracture without unduly decreasing

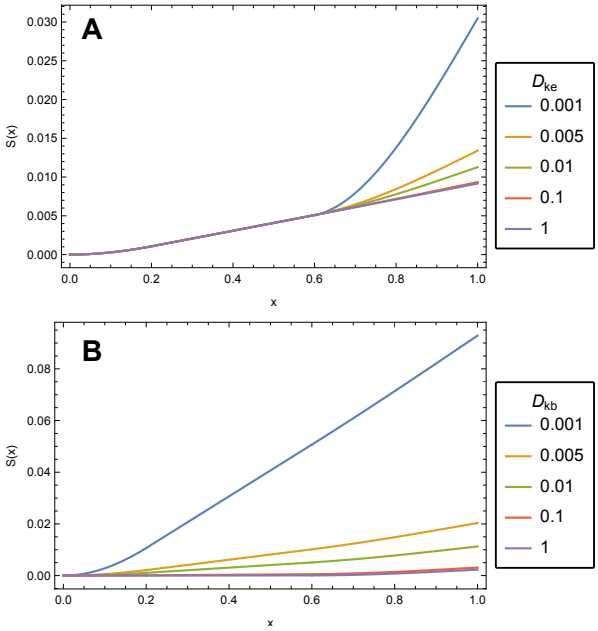

Figure 2.5: Deformation under an applied force for different values of the stiffness coefficients with fixed kerfed and pressed area lengths: $x_1 = 0.2$, $x_2 = 0.6$, $D_p = 2$, $L = 1$, and $F = -0.001$. (A) varying edge stiffness $D_{kb} = 0.01$; (B) varying base stiffness $D_{ke} = 0.01$.

the flexibility of the tube.

These results suggest that improvements to the flexibility can best be achieved either by increasing the proportion of the tube circumference occupied by the kerfed region at the base, that is increasing x_1, or by using a finer kerf pattern to decrease the stiffness D_{kb} through the base.

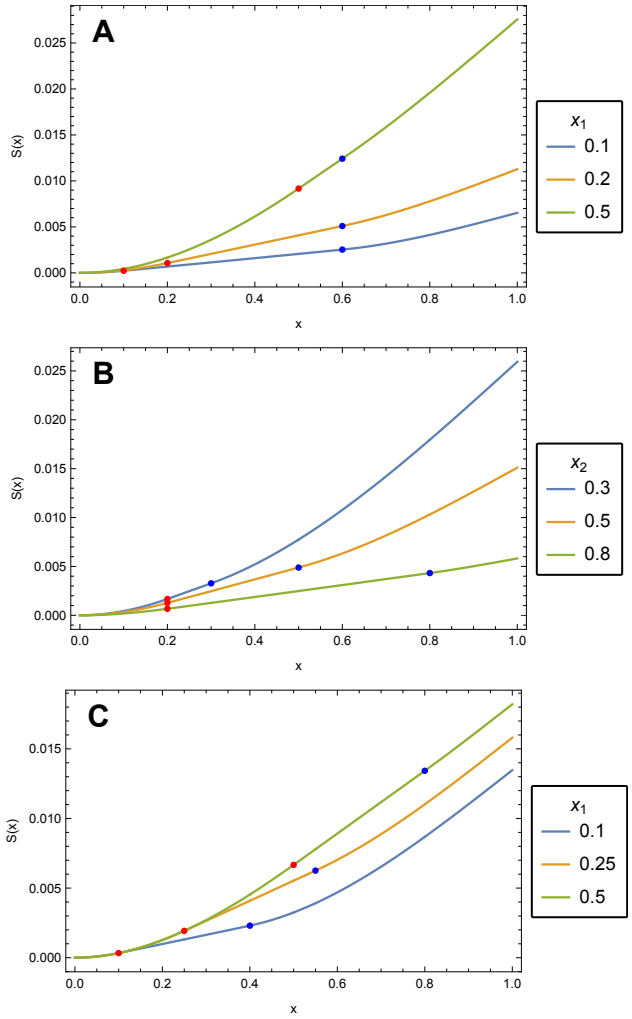

Figure 2.6: Deformation under an applied force for different lengths of the kerfing sections. The red dot indicates the edge of the base kerfing, and the blue dot indicates the start of the edge kerfing. (A) fixed edge kerfing length: $x_2 = 0.6$ with x_1 varying; (B) fixed base kerfing length: $x_1 = 0.2$ with x_2 varying; (C) fixed pressed region length: $x_2 = x_1 + 0.3$. All plots use $F = -0.001$, $L = 1$, $D_p = 2$, and $D_{kb} = D_{ke} = 0.01$.

3 A variational model for metal folding

The elastic deformation of a steel sheet after an initial plastic deformation can be modelled. Define a three dimensional Cartesian space with orthogonal basis coordinates (x, y, z), and assume that the steel begins as a flat sheet in the xz-plane with initial dimensions $0 \leqslant x \leqslant L$, and $0 \leqslant z \leqslant M$. The plastic and elastic deformations are assumed to produce a shape with translational symmetry in the z-direction, so that it is only necessary to consider the profile (plane curve) in the xy-plane.

After the initial plastic deformation, the sheet is assumed to have a prescribed shape given by $\mathbf{x} = (x_0(s), y_0(s))$, where s is arc length. In this section x_0 and y_0 are functions of the arclength that describe the shape of the deformed steel sheet in the xy-plane. This usage of these variables is distinct from the use of these symbols elsewhere in this report. Denote the signed curvature of $\mathbf{x}$ in the xy-plane by $k_0(s)$. This can be calculated from a given shape by estimating the first and second derivatives of x_0 and y_0 with respect to s, so that

$$k_0(s) = \dot{x}_0 \ddot{y}_0 - \ddot{x}_0 \dot{y}_0, \tag{3.1}$$

where dots denote differentiation with respect to s.

The other major material component of the model is the rigidity of the steel sheet. Assume an initial rigidity given by γ_{steel}, but note that the steel sheet is also decorated with kerfing patterns that modify the rigidity. Therefore, the material has a variable rigidity $\gamma(s)$ where γ depends on the arc length, s, due to the kerfing of the sheet. An example of $\gamma(s)$ is a periodic cosine function, which we adopt in Section 3.3 to demonstrate the results of the modelling.

3.1 Model

The elastic energy per unit length (in the z-direction) for the elastic deformation is given by the integral,

$$E = \int_0^L \gamma(s)\,(k(s) - k_0(s))^2\,ds, \tag{3.2}$$

where k denotes the signed curvature of the deformed curve. The calculus of variations can be used to determine the plane curve that gives a minimum value for (3.2).

The post-deformation curve can be parameterised using standard plane polar coordinates $(r(s), \theta(s))$, where again r and θ are functions of the arc length, s. In this form the signed curvature $k(s)$ is given by

$$k(s) = r(\dot{r}\ddot{\theta} - \ddot{r}\dot{\theta}) + \dot{\theta}(1 + \dot{r}^2). \tag{3.3}$$

We expect a curve that is approximately circular and thus adopt the endpoint conditions $r(0) = r(L) = L/(2\pi)$, $\theta(0) = 0$, and $\theta(L) = 2\pi$. Furthermore, assume the slope of the curve at the endpoints is vertical and therefore $\dot{r}(0) = \dot{r}(L) = 0$, and $\dot{\theta}(0) = \dot{\theta}(L) = 2\pi/L$.

The arc length parameterisation provides the identity,

$$\dot{r}^2 + r^2\dot{\theta}^2 = 1, \tag{3.4}$$

and assuming the curve is roughly circular then $\dot{\theta} > 0$ and $\dot{r} \ll 1$, and from (3.4),

$$\dot{\theta} = \frac{\sqrt{1 - \dot{r}^2}}{r}, \tag{3.5}$$

the differentiation of which gives,

$$\ddot{\theta} = \frac{\dot{r}(\dot{r}^2 - r\ddot{r} - 1)}{r^2\sqrt{1 - \dot{r}^2}}. \tag{3.6}$$

Substituting (3.5) and (3.6) into (3.3) leads to

$$k(s) = \frac{\dot{r}^2(\dot{r}^2 - r\ddot{r} - 1)}{r\sqrt{1-\dot{r}^2}} - \ddot{r}\sqrt{1-\dot{r}^2} + \frac{(1+\dot{r}^2)\sqrt{1-\dot{r}^2}}{r}. \tag{3.7}$$

Since $\dot{r} \ll 1$, a Maclaurin series for $k(s)$ in terms of $\dot{r}$ can be obtained as,

$$k(s) = \frac{1}{r} - \ddot{r} - \frac{1}{2}\left(\frac{1}{r} + \ddot{r}\right)\dot{r}^2 + \mathcal{O}(\dot{r}^4). \tag{3.8}$$

Note that (3.8), although easier to work with than (3.3), will not lead to a tractable Euler–Lagrange equation. Therefore, we consider an approximation to the signed-curvature based on the expectation of an almost circular solution curve.

3.2 Approximation for curvature

Since the resultant curve is expected to be close to circular, it is reasonable to assume that the x and y coordinates take the form,

$$x = r(s)\cos(\theta(s)), \quad y = r(s)\sin(\theta(s)),$$

and note that if the curve is a circle, $r(s) = r_0$ and $\theta(s) = s/r_0$. Adding small perturbations to these functions, denoted by $\epsilon r_1(s)$, and $\mu\theta_1(s)$, then

$$\begin{aligned} r(s) &= r_0 + \epsilon r_1(s) + \mathcal{O}(\epsilon^2), \\ \theta(s) &= \frac{s}{r_0} + \mu\theta_1(s) + \mathcal{O}(\mu^2), \end{aligned}$$

where $r_0 = L/(2\pi)$ is the ideal circular radius for a curve of length L, and $\epsilon, \mu \ll 1$. Differentiating with respect to s leads to

$$\dot{r} = \epsilon\dot{r}_1, \quad \ddot{r} = \epsilon\ddot{r}_1, \quad \dot{\theta} = \frac{1}{r_0} + \mu\dot{\theta}_1, \quad \ddot{\theta} = \mu\ddot{\theta}_1, \tag{3.9}$$

and hence from (3.4),

$$\epsilon^2 \dot{r_1}^2 + (r_0 + \epsilon r_1)^2 \left(\frac{1}{r_0} + \mu \dot{\theta}_1 \right)^2 = 1. \tag{3.10}$$

Expanding and retaining only terms up to first order in ϵ and μ, gives

$$1 + \epsilon \frac{2}{r_0} r_1 + \mu 2 r_0 \dot{\theta}_1 + \mathcal{O}(\epsilon^2, \mu^2, \epsilon\mu) = 1,$$

which leads to the approximate identity,

$$\mu \dot{\theta}_1 = -\epsilon \frac{r_1}{r_0^2}, \tag{3.11}$$

and hence,

$$\dot{\theta} = \frac{1}{r_0} - \epsilon \frac{r_1}{r_0^2}, \tag{3.12}$$

$$\ddot{\theta} = -\epsilon \frac{\dot{r}_1}{r_0^2}. \tag{3.13}$$

Employing (3.12) and (3.13) in the signed curvature (3.3), $k(s)$ becomes

$$k(s) = \frac{1}{r_0} - \epsilon \frac{r_1}{r_0^2} - \epsilon \ddot{r_1} + \mathcal{O}(\epsilon^2). \tag{3.14}$$

Thus, in terms of the original function r and the constant r_0,

$$k \approx \frac{2}{r_0} - \frac{1}{r_0^2} r - \ddot{r}, \tag{3.15}$$

and so it is possible to find the approximate functional as

$$E = \int_0^L \gamma(s) \left[\frac{2}{r_0} - \frac{1}{r_0^2} r - \ddot{r} - k_0(s) \right]^2 ds. \tag{3.16}$$

Recalling that $r_0 = L/(2\pi)$ and rescaling the problem such that $S = s/r_0$, $R(S) = r/r_0$, $\Gamma(S) = \gamma/r_0$ and $K_0(S) = r_0 k_0 - 2$, then

$$E = \int_0^{2\pi} \Gamma(S)\,[R''(S) + R(S) + K_0(S)]^2\,dS, \tag{3.17}$$

with

$$R(0) = R(2\pi) = 1, \quad R'(0) = R'(2\pi) = 0, \tag{3.18}$$

where primes denote differentiation with respect to S. Note that $\Theta(S) = \theta(s)$ has not been scaled, but the notation is adopted for consistency. Using $r = r_0 + \epsilon r_1$ gives $R = 1 + \epsilon r_1/r_0$ and (3.5), gives $\Theta' = 1 - \epsilon r_1/r_0$ and therefore the relationship

$$\Theta' = 2 - R, \tag{3.19}$$

can be used to determine $\Theta(S)$. Assuming that R remains in an ϵ-neighbourhood of 1, then the initial condition $\Theta(0) = 0$ should lead to $\Theta(2\pi) \approx 2\pi$, although it is not possible to impose this end condition.

In order to derive the Euler–Lagrange equation for this problem, note that the scaled integrand from (3.17) is given by

$$F(S, R, R', R'') = \Gamma(S)[R''(S) + R(S) + K_0(S)]^2, \tag{3.20}$$

which has the property that

$$\frac{\partial F}{\partial R} = \frac{\partial F}{\partial R''} = 2\Gamma(S)[R''(S) + R(S) + K_0(S)], \tag{3.21}$$

and therefore the Euler–Lagrange equation is of the form

$$\Phi'' + \Phi = 0, \tag{3.22}$$

where $\Phi(S) = \Gamma(S)[R''(S) + R(S) + K_0(S)]$. Putting to one side trivial cases (that should not apply in this case), it is possible to integrate (3.22) twice and derive the second-order equation

$$R''(S) + R(S) = \frac{1}{\Gamma(S)}\,(C_1 \cos S + C_2 \sin S) - K_0(S), \tag{3.23}$$

where C_1 and C_2 are arbitrary constants of integration. Further progress depends on the form of $\Gamma(S)$ and $K_0(S)$, which determine the particular solution of (3.23). Finally, note that in dimensional variables (3.23) is given by

$$\ddot{r} + \frac{4\pi^2}{L^2} r = \frac{1}{\gamma(s)} \left[C_1 \cos\left(\frac{2\pi s}{L}\right) + C_2 \sin\left(\frac{2\pi s}{L}\right) \right] + \frac{4\pi}{L} - k_0(s), \quad (3.24)$$

for which a solution can be written down involving integrals via the method of variation of parameters. However, the utility of that exercise depends on whether the resulting integrals are tractable, which again depends on the form of $\Gamma(S)$ and $K_0(S)$.

3.3 Results

To demonstrate a solution obtained from this approximate model, consider the case of constant rigidity and initial curvature given by the trimodal function

$$K_0(S) = -1 + \frac{1}{2}\cos 3S.$$

Imposing the boundary conditions $R(0) = R(2\pi) = 0$, gives

$$R(S) = 1 + \frac{1}{16}(\cos 3S - \cos S) + \left(C_4 - \frac{3}{4}\right) S \sin S + C_2 \sin S.$$

Choosing $C_4 = 3/4$ to remove the secular term and $C_2 = 0$ so that $R'(0) = R'(2\pi) = 0$, gives

$$R(S) = 1 + \frac{1}{16}(\cos 3S - \cos S). \quad (3.25)$$

Using this value of R and $\Theta(0) = 0$ in (3.19) gives in this case,

$$\Theta(S) = S + \frac{1}{12}\sin^3 S. \quad (3.26)$$

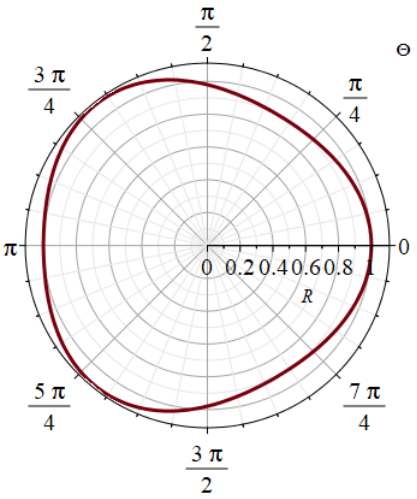

Figure 3.1: Solution of nondimensionalised problem with constant Γ and trimodal $K_0(S)$ inputs.

A plot of this solution is shown in Figure 3.1.

Note that Figure 3.1 is only to demonstrate an example of using the model and that the figure does not match the configuration shown in Figure 2.2d. In order to use this model for the SuTiT, further study would be required to determine appropriate choices for $\Gamma(S)$ and $K_0(S)$, which in turn depend on the kerfing pattern.

4 A static equilibrium model of kerfing patterns under stress

To understand the forces through the kerfing pattern as the liner is bent into the tube, it is necessary to develop a simplified static equilibrium model of kerfing patterns under stress. The kerfing pattern is modelled as a series of

beams connected at nodes, see Figure 4.1. Let the x direction be the long edge of the SuTiT, with the positive direction being to the right, and the y direction be the short edge, with the positive direction being away from the short edge. Let an arbitrary node be given by (i, j) where i is the x index and j is the y index, and the angle between the nodes (i, j) and $(i, j+1)$ be given by ϕ. Also assume that there are only angles in the y-direction and that all angles are the same, i.e. all lines in the x direction run parallel to the long edge and all lines in the y-direction are parallel. Finally, denote the force along the beam between nodes (i, j) and $(i, j+1)$ as $f_{i,j+\frac{1}{2}}$.

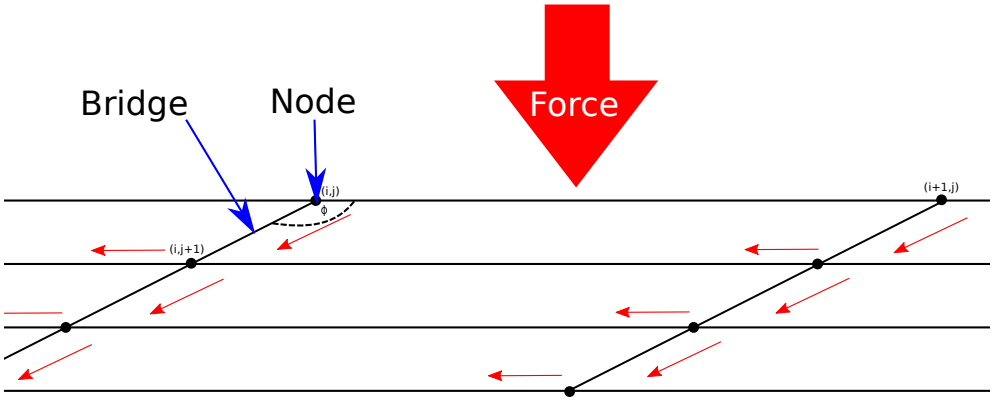

Figure 4.1: Method of static equilibrium. The force occurring over the bridge is increased proportional to the angle between bridges. If the bridges are offset a twisting force is induced.

In this model, a force, F, is applied evenly to the nodes on the long edge of the SuTiT in order to bend and hold it in shape. As the SuTiT is at equilibrium, the force at each node must equal zero in both the x and y directions. Therefore, the forces at a node in the x-direction in the first row and an arbitrary node $j > 1$ are,

$$(i, 1) \ : f_{i-\frac{1}{2},1} - f_{i+\frac{1}{2},1} - f_{i,1+\frac{1}{2}} \cos\phi = 0,$$

$$(i,j) \ : f_{i-\frac{1}{2},j} - f_{i+\frac{1}{2},j} - f_{i,j-\frac{1}{2}} \cos\phi - f_{i,j+\frac{1}{2}} \cos\phi = 0,$$

and similarly, for the y-direction,

$$\begin{aligned}(i,1) \ &: F - f_{i,1+\frac{1}{2}} \sin\phi = 0,\\ (i,j) \ &: f_{i,j-\frac{1}{2}} \sin\phi - f_{i,j+\frac{1}{2}} \sin\phi = 0.\end{aligned}$$

The forces along beams in the y-direction are therefore

$$f_{i,1+\frac{1}{2}} = \frac{F}{\sin\phi} \rightarrow f_{i,j-\frac{1}{2}} = \frac{F}{\sin\phi},$$

and the forces along the beams in the x-direction are

$$f_{i-\frac{1}{2},j} - f_{i+\frac{1}{2},j} = 2\frac{F\cos\phi}{\sin\phi}.$$

This model shows that the angle between successive bridges, ϕ, is vital for minimising the stress at the connection points, which have been observed to fracture. Bridges arranged in lines at an angle to the applied force experience a twisting force, increasing their fracture risk. To counter this, bridges should be arranged in lines perpendicular to the applied force, that is, parallel to the short axis of the SuTiT, although this will make the SuTiT slightly harder to bend.

5 Elasticity model

The combined linear elastic-plasticity problem of deforming a thin rectangular sheet of metal to an almost complete circular cylindrical tube is unsolved because it involves a complicated coupling of the displacement and stress boundary-value problems. Even the linear elastic problem in isolation remains unsolved, and the best that might be expected is to obtain a stress field that is approximately consistent with the major deformation characteristics, and this is the problem that is attempted in this section. A linear elastic

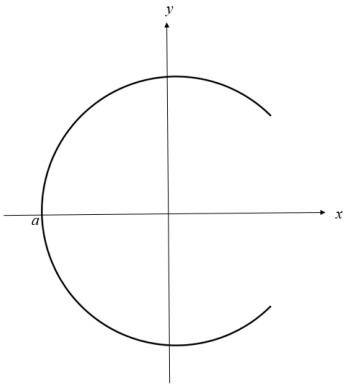

Figure 5.1: Cross section of an almost completed circular cylinder.

stress field that is compatible with the expected deformation is obtained and used to investigate the possible stress boundary-value problems. The interesting aspect of the analysis arises from the assumption that there is no circumferential extension, which singles out stress fields that do not arise from a classical linear elastic analysis.

Suppose that a long thin rectangular metal plate of width $2\pi a$ has as its original configuration that of an almost complete circular cylinder, the cross-section of which is shown in Figure 5.1. Consider the linear elastic problem of deformation to a complete right circular cylinder with the additional assumptions,

i. the problem may be viewed as one of plane strain,

ii. the plate is sufficiently thin so that any boundary conditions apply along the single curve $r = a$,

iii. the x-axis is a line of symmetry,

iv. there is no circumferential extension,

v. the point-wise stress boundary condition of an applied all-round uniform

pressure may be approximated by averages over the upper and lower area.

Assumption (iv) implies that with original and final coordinates (r, θ) and (r', θ') respectively, then inextensibility along the circumference gives

$$r' d\theta' = r d\theta,$$

and therefore assuming that

$$r' = r + u(r, \theta), \quad \theta' = \theta + v(r, \theta), \tag{5.1}$$

gives

$$r d\theta = (r + u(r, \theta))(d\theta + dv(r, \theta)), \tag{5.2}$$

or to first order,

$$u d\theta + r\left(\frac{\partial u}{\partial r} dr + \frac{\partial v}{\partial \theta} d\theta\right) = 0.$$

Along $r = a$,

$$u(r, \theta) = -r \frac{\partial v(r, \theta)}{\partial \theta}, \tag{5.3}$$

noting that in linear elasticity there is no essential difference between undeformed and deformed coordinates and that (5.3) provides an important simplification.

The general plane strain equations (Fung [1]) for stresses and strains are,

$$\varepsilon_{rr} = \frac{\partial u}{\partial r}, \quad \varepsilon_{\theta\theta} = \frac{\partial v}{\partial \theta} + \frac{u}{r}, \quad \varepsilon_{r\theta} = \frac{1}{2}\left(\frac{1}{r}\frac{\partial u}{\partial \theta} + rv\right), \tag{5.4}$$

noting that Fung [1] uses the physical displacements $\xi_r = u$ and $\xi_\theta = rv$. In plane strain,

$$\begin{aligned} \varepsilon_{rr} &= \frac{(1+\nu)}{E}\{(1-\nu)\sigma_{rr} - \nu\sigma_{\theta\theta}\}, \\ \varepsilon_{\theta\theta} &= \frac{(1+\nu)}{E}\{(1-\nu)\sigma_{\theta\theta} - \nu\sigma_{rr}\}, \end{aligned} \tag{5.5}$$

$$\varepsilon_{r\theta} = \frac{(1+\nu)}{E}\sigma_{r\theta},$$

where E is Young's modulus and ν is Poisson's ratio. Further, the stress equilibrium equations with no body forces are,

$$\frac{\partial(r\sigma_{rr})}{\partial r} + \frac{\partial \sigma_{r\theta}}{\partial \theta} - \sigma_{\theta\theta} = 0, \tag{5.6}$$

$$\frac{1}{r}\frac{\partial(r^2\sigma_{r\theta})}{\partial r} + \frac{\partial \sigma_{\theta\theta}}{\partial \theta} = 0. \tag{5.7}$$

Denoting $A = \sigma_{rr}$, $B = \sigma_{r\theta}$ and $C = \sigma_{\theta\theta}$ then from (5.3), $\varepsilon_{\theta\theta} = 0$ and so $(1-\nu)C = \nu A$ and the relations (5.4) and (5.5) give

$$\frac{\partial u}{\partial r} = \frac{(1+\nu)(1-2\nu)}{E(1-\nu)}A, \tag{5.8}$$

$$\frac{1}{r}\frac{\partial u}{\partial \theta} = \frac{2(1+\nu)}{E}B - r\nu, \tag{5.9}$$

and from (5.6) and (5.7),

$$r\frac{\partial A}{\partial r} + \frac{(1-2\nu)}{(1-\nu)}A + \frac{\partial B}{\partial \theta} = 0, \tag{5.10}$$

$$r\frac{\partial B}{\partial r} + 2B + \frac{\nu}{(1-\nu)}\frac{\partial A}{\partial \theta} = 0, \tag{5.11}$$

which can be solved as two equations for the unknowns A and B. Multiplying the first equation by $\nu/(1-\nu)$ and differentiating with respect to θ to eliminate A, gives

$$r\frac{\partial}{\partial r}\left\{r\frac{\partial B}{\partial r} + 2B\right\} + \frac{(1-2\nu)}{(1-\nu)}\left\{r\frac{\partial B}{\partial r} + 2B\right\} - \frac{\nu}{(1-\nu)}\frac{\partial^2 B}{\partial \theta^2} = 0, \tag{5.12}$$

which becomes

$$(1-\nu)r^2\frac{\partial^2 B}{\partial r^2} + (4-5\nu)r\frac{\partial B}{\partial r} + 2(1-2\nu)B - \nu\frac{\partial^2 B}{\partial \theta^2} = 0. \tag{5.13}$$

This can be simplified to give

$$(1-\nu)\left(r^2B\right)_{rr} - \frac{\nu}{r}\left(r^2B\right)_r - \nu B_{\theta\theta} = 0, \tag{5.14}$$

or with $D = r^2B$,

$$(1-\nu)D_{rr} - \frac{\nu}{r}D_r - \frac{\nu}{r^2}D_{\theta\theta} = 0. \tag{5.15}$$

Introducing the notation $\beta = \nu/(1-\nu)$ then (5.15) becomes

$$D_{rr} - \frac{\beta}{r}D_r - \frac{\beta}{r^2}D_{\theta\theta} = 0, \tag{5.16}$$

where since $0 \leqslant \nu \leqslant 1/2$, it is true that $0 \leqslant \beta \leqslant 1$.

Equation (5.16), has a separable solution of the form $D(r,\theta) = F(r)G(\theta)$, which upon substitution leads to

$$\frac{r^2}{F(r)}\left\{F''(r) - \frac{\beta}{r}F'(r)\right\} = \beta\frac{G''(\theta)}{G(\theta)} = -\beta\lambda^2, \tag{5.17}$$

so that $G'' + \lambda^2 G = 0$ and $G(\theta) = \sin\lambda\theta$. Substituting $F(r) = r^m$, then $m^2 - (\beta+1)m + \beta\lambda^2 = 0$, and

$$m = \frac{(\beta+1) \pm \sqrt{(\beta+1)^2 - 4\beta\lambda^2}}{2}. \tag{5.18}$$

If $\lambda = n$ (an integer) then for $0 \leqslant \beta \leqslant 1$, only $n = 1$ produces two real roots. For $n \geqslant 2$ we have

$$m_1 = \frac{1}{2}(\beta+1) + im, \quad m_2 = \frac{1}{2}(\beta+1) - im, \tag{5.19}$$

where

$$m = \frac{1}{2}\left[4\beta n^2 - (\beta+1)^2\right]^{1/2}. \tag{5.20}$$

If $n = 1$, $m_1 = 1$, $m_2 = \beta$ and $\sigma_{r\theta}(a,\theta) = 0$ then

$$\sigma_{r\theta} = B = \frac{D}{r^2} = C_1\left[\frac{a}{r} - \left(\frac{a}{r}\right)^{2-\beta}\right]\sin\theta, \tag{5.21}$$

and for general n, $\sigma_{r\theta}(a,\theta) = 0$ gives

$$\sigma_{r\theta} = B = \frac{D}{r^2} = C_n r^{\frac{1}{2}(\beta+1)-2} \sin\left(m \log(r/a)\right) \sin n\theta. \tag{5.22}$$

Now it is possible to determine $A = \sigma_{rr}$ from (5.11),

$$\frac{\partial A}{\partial \theta} = -\frac{1}{\beta r}\frac{\partial D}{\partial r}, \tag{5.23}$$

and thus for $n = 1$,

$$\sigma_{rr} = A = \frac{C_1}{a}\left[\frac{1}{\beta}\left(\frac{a}{r}\right) - \left(\frac{a}{r}\right)^{2-\beta}\right]\cos\theta, \tag{5.24}$$

while for general $n \geqslant 1$,

$$\sigma_{rr} = A = \frac{C_n}{\beta n} r^{(\beta-3)/2}\left\{\frac{(\beta+1)}{2}\sin\left[m\log\left(\frac{r}{a}\right)\right] + m\cos\left[m\log\left(\frac{r}{a}\right)\right]\right\}\cos n\theta. \tag{5.25}$$

Assuming a constant all-round pressure P along $r = a$, the point-wise boundary condition is $\sigma_{rr}(a,\theta) = -P$, then for the Fourier cosine series

$$A_0 + \frac{C_1}{\beta a^2}(a^2 - \beta)\cos\theta + \sum_{n=2}^{\infty} \frac{C_n a^{(\beta+1)/2}}{2\beta n a^2}\left[4\beta n^2 - (\beta+1)^2\right]^{1/2}\cos n\theta = -P, \tag{5.26}$$

the coefficients are,

$$A_0 = -\frac{1}{\pi}\int_0^{\pi} P\,d\theta = -P, \tag{5.27}$$

$$A_n = -\frac{2}{\pi}\int_0^{\pi} P\cos n\theta\,d\theta = -\frac{2}{\pi}P\left[\frac{\sin n\theta}{n}\right]_0^{\pi} = 0, \tag{5.28}$$

for $\frac{A_0}{2} + \sum_{n=1}^{\infty} A_n \cos n\theta$, and therefore with this particular solution, we cannot represent a constant all-round applied pressure with a non-trivial Fourier

cosine series. However, we exploit the solution for $n = 1$ to determine an approximate solution for which an average replaces the point-wise pressure boundary condition, namely

$$\int_0^\pi \sigma_{rr}(a,\theta)\sin\theta a\,d\theta = \int_0^\pi P\sin\theta a\,d\theta = 2Pa, \tag{5.29}$$

and for $\lambda = n = 1$, it is necessary that $v(a,0) = v(a,2\pi) = 0$, and then the stronger pressure boundary condition can be satisfied by

$$\int_0^\alpha \sigma_{rr}(a,\theta)\sin\theta a\,d\theta = \int_0^\alpha P\sin\theta a\,d\theta = Pa(1-\cos\alpha), \tag{5.30}$$

for arbitrary angle α.

In summary, for the single term approximate solution arising from $\lambda = n = 1$, with $m_1 = 1$ and $m_2 = \beta$, where $\beta = \nu/(1-\nu)$, there are two constants C_1 and C_2 that are determined by $\sigma_{r\theta}(a,\theta) = 0$, while the point-wise condition on $\sigma_{rr}(a,\theta)$ is replaced by the above average requirement (5.30). The final stresses and displacements are then given by

$$\begin{aligned}
\sigma_{rr} &= \frac{P^*}{\beta}\left[\frac{a}{r} - \beta\left(\frac{a}{r}\right)^{2-\beta}\right]\frac{\cos\theta}{(1-\beta)},\\
\sigma_{r\theta} &= P^*\left[\frac{a}{r} - \left(\frac{a}{r}\right)^{2-\beta}\right]\frac{\sin\theta}{(1-\beta)},\\
\sigma_{\theta\theta} &= P^*\left[\frac{a}{r} - \beta\left(\frac{a}{r}\right)^{2-\beta}\right]\frac{\cos\theta}{(1-\beta)},
\end{aligned}$$

and

$$\begin{aligned}
u(r,\theta) &= \frac{(1+r)aP^*}{E\beta}\left\{\left[\log\left(\frac{r}{a}\right) + \frac{\beta}{1-\beta}\left(\frac{a}{r}\right)^{1-\beta}\right]\cos\theta + \frac{\beta}{1-\beta}\right\},\\
v(r,\theta) &= -\frac{(1+r)aP^*}{E\beta}\left\{\left[\log\left(\frac{r}{a}\right) + \frac{\beta}{1-\beta}\left(\frac{a}{r}\right)^{1-\beta}\right]\frac{\sin\theta}{r} + \frac{\beta(\theta-\pi)}{1-\beta}\right\},
\end{aligned}$$

where $P^* = \beta P/\cos\alpha$, and the additive constants are chosen so that $u(a,\pi) = v(a,\pi) = 0$.

The general linear elastic solution arises as a solution of the bi-harmonic equation, usually in cylindrical polar coordinates. The above approximate solution is interesting because solutions involving r^{β} are not embodied directly in the general solution, and it arises as a consequence of the circumferential inextensibility of the tube.

6 Conclusions

Several models have been proposed and implemented to study the design of the inner tube in the core sampler. As a result of this work it is the conclusion of the study group that the strength and durability of the SuTiT could be improved by exploring the following:

- The kerfed region at the edges results in a near-linear shape while adding little to the tube's flexibility. CarbonPump should consider increasing the width of the kerfed region at the base and use cold presses to obtain the circular shape.
- Bridges arranged in lines at an angle to the applied force introduce a twisting force at the bridges. CarbonPump should consider using kerf patterns where the bridges are perpendicular to the applied force.
- A trade-off exists between flexibility and strength. CarbonPump should seek to minimise the amount of material removed (number of cuts) to achieve no more flexibility than required. Our models suggest a laser cut length reduction of 50% will maintain appropriate elasticity for outer tube insertion and reduce manufacturing costs.

Acknowledgements

We thank the industry representatives Ignatius Verbeek and Stuart Morris for their contributions to the discussion and direction of this study throughout the study group. We also thank Bishnu Lamichhane and Graeme Hocking for their insightful discussions on this project.

References

[1] Y. C. Fung. *Foundations of Solid Mechanics*. Prentice Hall, 1969.

[2] Cole D. Gross and Robert B. Harrison. Quantifying and comparing soil carbon stocks: Underestimation with the core sampling method. *Soil Science Society of America Journal*, 82(4):949–959, July 2018.

[3] E. I. Vanguelova, E. Bonifacio, B. De Vos, M. R. Hoosbeek, T. W. Berger, L. Vesterdal, K. Armolaitis, L. Celi, L. Dinca, O. J. Kjønaas, P. Pavlenda, J. Pumpanen, Ü. Püttsepp, B. Reidy, P. Simončič, B. Tobin, and M. Zhiyanski. Sources of errors and uncertainties in the assessment of forest soil carbon stocks at different scales—review and recommendations. *Environmental Monitoring and Assessment*, 188(11), October 2016.

Author addresses

1. **Melanie E. Roberts**, Australian Rivers Institute, Griffith University, Australia.
mailto:m.roberts2@griffith.edu.au
orcid:0000-0003-4027-9651

2. **Fillipe Georgiou**, School of Information and Physical Sciences, University of Newcastle, Callaghan, NSW 2308, Australia.
mailto:fillipe.georgiou@uon.edu.au
orcid:0000-0003-4588-5319

3. **Edward J Bissaker**, School of Information and Physical Sciences, University of Newcastle, Australia.
mailto:edward.bissaker@uon.edu.au
orcid:0000-0002-1608-286X

4. **Barry J. Cox**, School of Mathematical Sciences, University of Adelaide, Adelaide, SA 5005, Australia.
mailto:barry.cox@adelaide.edu.au
orcid:0000-0002-0662-7037

5. **James M. Hill**, School of Information Technology and Mathematical Sciences, University of South Australia, GPO Box 2471, Adelaide, SA 5001, Australia.
mailto:jim.hill@unisa.edu.au
orcid:0000-0003-4623-2811

6. **Michael H. Meylan**, School of Information and Physical Sciences, University of Newcastle, Callaghan, NSW 2308, Australia.
mailto:mike.meylan@newcastle.edu.au
orcid:0000-0002-3164-1367

7. **Josiah Murray**, School of Information and Physical Sciences, University of Newcastle, Australia
mailto:josiah.murray@uon.edu.au
orcid:0000-0002-8060-911X

8. **Winston L. Sweatman**, School of Mathematical and Computational Sciences, Massey University, Auckland, New Zealand.
mailto:w.sweatman@massey.ac.nz
orcid:0000-0002-6540-5020

9. **Ngamta Thamwattana**, School of Information and Physical Sciences, University of Newcastle, Callaghan, NSW 2308, Australia.
mailto:natalie.thamwattana@newcastle.edu.au
orcid:0000-0001-9885-3287